

Collective charge excitations between moiré-minibands in twisted WSe₂ bilayers from resonant inelastic light scattering

Nihit Saigal,¹ Lennart Klebl,² Hendrik Lambers,¹ Sina Bahmanyar,¹ Veljko Antić,¹ Dante M. Kennes,^{3,4} Tim O. Wehling,^{2,5} and Ursula Wurstbauer^{1,6}

¹*Institute of Physics, University of Münster, Wilhelm-Klemm-Str. 10, 48149 Münster, Germany*

²*Institute of Theoretical Physics, University of Hamburg, Notkestrasse 9, 22607 Hamburg, Germany*

³*Institute for Theory of Statistical Physics, RWTH Aachen University, and JARA Fundamentals of Future Information Technology, 52062 Aachen, Germany*

⁴*Max Planck Institute for the Structure and Dynamics of Matter, Center for Free Electron Laser Science, 22761 Hamburg, Germany*

⁵*The Hamburg Centre for Ultrafast Imaging, 22761 Hamburg, Germany*

⁶*Center for Soft Nanoscience (SoN), Busso-Peus-Str. 10, 48149 Münster, Germany**

(Dated: June 17, 2024)

We establish low-temperature resonant inelastic light scattering (RILS) spectroscopy as a tool to probe the formation of a series of moiré-bands in twisted WSe₂ bilayers by accessing collective inter-moiré-band excitations (IMBE). We observe resonances in RILS spectra at energies in agreement with inter-moiré band transitions obtained from an *ab-initio* based continuum model. Transitions between the first and second inter-moiré band for a twist angle of about 8° are reported and between first and second, third and higher bands for a twist of about 3°. The signatures from IMBE for the latter highlight a strong departure from parabolic bands with flat minibands exhibiting very high density of states in accord with theory. These observations allow to quantify the transition energies at the K-point where the states relevant for correlation physics are hosted.

Twisted van der Waals (vdW) bilayers present a unique condensed matter platform to realize and control electronic correlation effects [1, 2, 4]. The large scale superlattice created by the superposition of the two layers at a slight rotational mismatch defines a reciprocal mini-Brillouin zone with nearly dispersionless (flat) bands as long as the layers hybridize sufficiently. The drastically reduced kinetic energy results in a very high density of states (DOS) and even van Hove physics in those bands, driving electrons into the correlated regime [4, 5]. In several graphene-based systems correlated and ordered electronic phases are experimentally well-established [6–10]. In transition metal dichalcogenide (TMDC) based vdW stacks the absence of complications like topological obstructions have facilitated high-level microscopic many-body studies from early on [11] and explained the emergence of ordered, insulating and also different flavors of correlated metallic states of matter [12, 13]. Experimentally, the aforementioned correlation effects have been realized [14, 15], while superconductivity has remained elusive with currently one report of an (unclear and controversial) zero resistance state [14] even though there are multiple theoretical studies [16–18].

These emergent phases in semiconductor-based moiré bilayers are attributed to strongly interacting electronic K/K'-states. In this letter, we experimentally access moiré minibands at the valence band maximum (VBM) around the K/K' valley by studying their collective electronic inter-moiré band excitations (IMBE) by

resonant inelastic light scattering (RILS) experiments as summarized in Fig. 1. Accessing the moiré bands at the K-points is challenging for the combined reason of twist angle variations and reconstruction in realistic devices together with the VBM at the Γ and K-points being close in energy [19]. The morphology of twisted bilayers, particularly at small twist angles, is such that variations in twist angle, but also reconstruction (in plane as well as corrugation) plays an important role. This leads to periodically patterned areas different to those expected from a rigid moiré lattice-picture [20–23]. While these patterns result in rich optical interband spectra [23] and even host coherent many-body states of excitons [24], it makes the interpretation of spectroscopic signatures and the direct spectroscopy of moiré bands e.g. by angle-resolved photoemission spectroscopy (ARPES) difficult with only a few reports on selected materials combinations [25, 26]. Recent μ -ARPES and STM studies demonstrate the formation of moiré-bands at the valence band maximum (VBM) at the Γ -point of twisted WSe₂ bilayers [22, 27, 28]. Accessing moiré bands around the K/K' states and their properties is still lacking.

We remedy this standing problem by reporting on collective electronic excitations between moiré bands formed in twisted and hBN encapsulated WSe₂ bilayers [Fig. 1(a,b)] at the VBM around the K/K' states. By combined theoretical and experimental efforts, we demonstrate that probing the moiré-bands via collective single-particle-like IMBE by RILS spectroscopy analogue to intersubband excitations in 2D charge carrier systems

* wurstbauer@uni-muenster.de

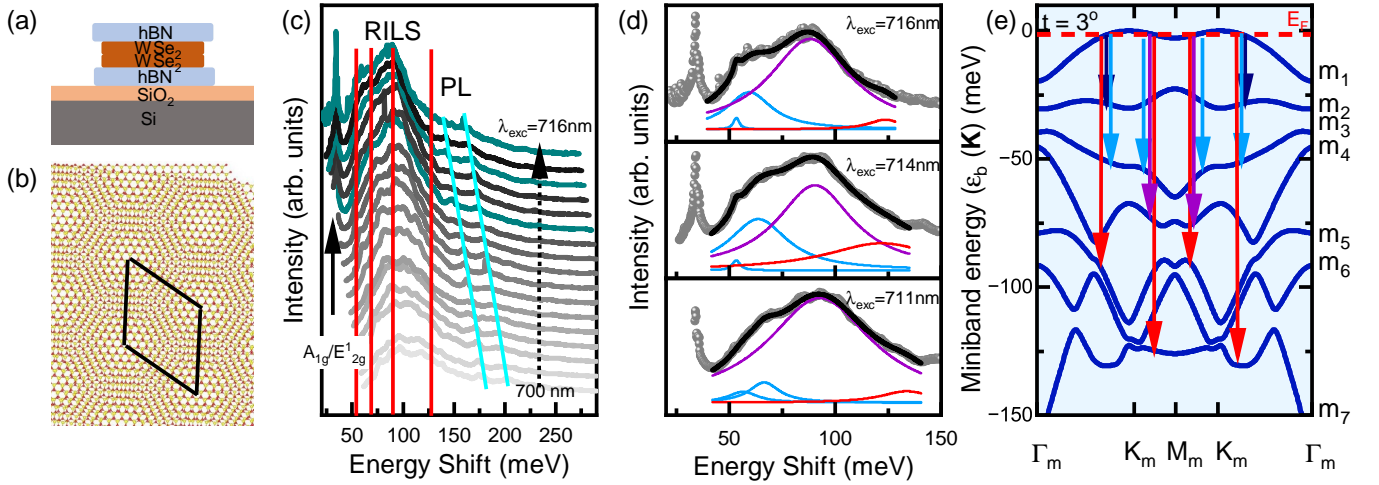


FIG. 1. (a) Scheme of the hBN encapsulated tWSe₂ bilayer. (b) Stick-ball model of a moiré superlattice from a tWSe₂ bilayer with the moiré unit cell indicated. (c) RILS spectra on a 3° tWSe₂ bilayer. Spectra are offset for clarity. The A_{1g}/E_{2g} phonons are indicated by a black solid arrow. The broad RILS signal are collective electronic inter-moiré band excitations (IMBE). The vertical red solid lines mark resonance energies from theoretically predicted transition energies. The tilted cyan lines indicate emission signatures. For the dark cyan spectra results from line-shape analysis are shown in (d) [T = 4K, P_{Laser} = 1 mW]. (d) Selected RILS spectra (data points) from (c). The solid lines are fit results, using a set of Lorentzian lines to numerically deconvolute the individual contribution from the RILS spectra. The black lines are the sum of all Lorentzian curves. (e) Calculated energy dispersion of the 7 highest moiré minibands around the K, K' states for a 3° tWSe₂ bilayer. The minibands are labelled m₁, m₂, ...m₇. Exemplary inter-miniband transitions are sketched.

hosted e.g. in GaAs quantum wells [29–31] provides a promising approach to study the band structure of twisted transition metal dichalcogenides at twist angles where correlation physics play an important role [4, 12, 13, 16–18].

The hBN encapsulated tWSe₂ bilayers have been prepared by micromechanical cleavage and viscoelastic dry transfer on top of Si/SiO₂ substrates with an estimated twist uncertainty of about ±0.5°. Three different types of WSe₂ samples have been prepared with a twist of 3°, 8° and a natural homobilayer. To check for sufficient interlayer coupling and twist angle we employ low-temperature non-resonant Raman and PL spectroscopy (see SI-Figs.1, 2 [32]). For all measurements, the samples are mounted on the cold-finger of a closed-cycle refrigerator at a temperature of T = 4K. Position control is provided by x-y-z piezo actuators. The light from either a green solid state laser (2.33 eV) or a continuously tunable Ti:sapphire laser (linewidth of about 50 kHz) is focused with a cryogenic large-NA (NA = 0.82) objective lens to spot size of less than 2μm. The emitted/scattered light is guided to the entrance slit of a triple grating spectrometer. In RILS experiments, the sample is excited by linearly polarized light in back-scattering geometry and the scattered light is unpolarized (see SI-Fig.6 for polarization dependent spectra [32]). Due to the large NA of the objective a distribution of in-plane momenta $q_{\parallel} < 2\omega_L/c \sin \theta_{\max}$ with $\theta_{\max} \approx 55^\circ$ is transferred to the hole system.

By excitation in resonance close to the direct optical allowed interband transition at the K/K'-point (A_{1s}-exciton), IMBEs at the K/K' VBM can be probed by low-temperature RILS spectroscopy. Typical RILS spectra taken on a $t \approx 3^\circ$ twisted WSe₂ bilayer at T = 4K are shown in a water fall representation in Fig. 1(c). The resonance excitation wavelengths are determined from PL experiments (see SI-Fig.1 [32]). A rich spectrum of rather wide and dispersive RILS modes (red lines) is accompanied by the sharp nearly degenerate optical active A_{1g}, E_{2g}¹ phonon modes at an energy range between 20 meV and 120 meV. In order to deconvolute individual contributions to the RILS spectra, we perform a line-shape analysis by fitting a sum of Lorentzian curves to the spectra. We first focus on the energy range between 40 meV and 130 meV. The RILS spectra for all excitation wavelengths used are well reproduced by a sum of four (five) Lorentz functions for larger and smaller wavelengths, respectively. The energetic positions of the individual terms stay nearly constant, while the intensities are affected by the resonance conditions. This finding strongly suggests that the observed RILS mode originate from scattering on collective electronic excitation in analogy to intersubband excitations in GaAs based low-dimensional structures [29, 33, 34]. We would like to note that the quantitative interpretation from a similar quantitative line-shape analysis in the 20 meV to 35 meV is challenging since at least 7 phonon modes under the chosen resonance conditions are reported in liter-

ature [8]. Superimposed to these phonon modes and PL background, an additional mode occurs under extreme resonance at the red tail A_{1g} , E_{2g}^1 phonon modes at an energy of about 28.8 meV (for a detailed analysis see SI-Fig.5 [32]). Due to its occurrence only under extreme resonance in contrast to the resonantly activated phonon modes, we assign this mode also to an electronic excitation.

The extracted mode energies are in good quantitative agreement with inter-moiré band transitions extracted from the calculated electronic bands in the mini-BZ (mBZ) in the vicinity of the K/K' points. For direct comparison, Fig. 1(e) summarizes the first seven moiré minibands with examples of vertical transitions starting from the Fermi surface in the highest moiré band m_1 . We obtain the band structures of tWSe₂ from a continuum model [4–7] with parameters adjusted to *ab-initio* simulations (for details see SI [32]).

We explain the observed RILS spectra by a three-step scattering process for IMBE of photo-generated holes following the concept well-established for single-particle intersubband excitations in GaAs-based films [29–31] and successfully applied to e.g. RILS on intersubband excitation of photo-generated electrons and holes in ultrathin GaAs-based nanowires [34]. Fig. S1(a) illustrates the scattering processes for the $m_1 \rightarrow m_2$ (left) and $m_1 \rightarrow m_3$ (right) transitions: In the first step an electron from a VB state at K/K' is excited to a virtual state close to the upper CB band at K/K' (spin allowed transition). If the virtual electronic state is just above the CB by the energy of an IMBE, in the second step, the electron can be resonantly scattered via Coulomb interaction with a hole in m_1 miniband at the (quasi) Fermi-level to the CB. Simultaneously, an IMBE (e.g. $m_1 \rightarrow m_2$) is created in the valence band. In the third step, the scattered electron-hole pair recombines under emission of the the scattered photon. The same concept applies by including excitonic effects (not included in the scheme for clarity). The experiment is done under cw excitation such that a plasma of photo-generated holes is forming a quasi Fermi-level in the topmost miniband due to quick relaxation. We assume a charge imbalance between electrons and holes at the K/K' valley since the WSe₂ is expected to be slightly hole-doped and in addition photo-generated electrons are supposed to relax into the energetically lower Σ -valley [39].

The hBN encapsulated tWSe₂ bilayers have been prepared by micromechanical cleavage and viscoelastic dry transfer on top of Si/SiO₂ substrates with an estimated twist uncertainty of about $\pm 0.5^\circ$. Three different types of WSe₂ samples have been prepared with a twist of 3° , 8° and a natural homobilayer. To check for sufficient interlayer coupling and twist angle we employ low-temperature non-resonant Raman and PL spectroscopy (see SI-Figs.1, 2 [32]). For all measurements, the samples

are mounted on the cold-finger of a closed-cycle refrigerator at a temperature of $T = 4\text{K}$. Position control is provided by x-y-z piezo actuators. The light from either a green solid state laser (2.33 eV) or a continuously tunable Ti:sapphire laser (linewidth of about 50 kHz) is focused with a cryogenic large-NA (NA = 0.82) objective lens to spot size of less than $2\mu\text{m}$. The emitted/scattered light is guided to the entrance slit of a triple grating spectrometer. In RILS experiments, the sample is excited by linearly polarized light in back-scattering geometry and the scattered light is unpolarized (see SI-Fig.6 for polarization dependent spectra [32]). Due to the large NA of the objective a distribution of in-plane momenta $q_{\parallel} < 2\omega_L/c \sin \theta_{\text{max}}$ with $\theta_{\text{max}} \approx 55^\circ$ is transferred to the hole system.

Since jDOS is dependent on E_F , complementary excitation-power dependent RILS measurements are done in order to vary E_F by the photo-induced holes from $\Delta p \approx 10^9 \text{cm}^{-2}$ to $\Delta p \approx 10^{10} \text{cm}^{-2}$ and $\Delta p \approx 10^{12} \text{cm}^{-2}$. Due to the strong band non-parabolicity and the unknown intrinsic doping it was not possible to estimate the change in E_F from Δp . In agreement with expectation from jDOS, the RILS intensities in the lower-energy region assigned to superimposed phonons and collective electronic excitations including the tentative IMBE $m_1 \rightarrow m_2$ is reduced, while the modes are enhanced with slight modification in their energies in line with expectations from theory (spectra and summary from line-shape analysis shown in SI-Figs.3,4 [32]).

In Fig.S1(b) we summarize IMBE-energies extracted from the lineshape analysis of the RILS spectra of the 3° tWSe₂ described above. The nominal numerical fit error is only a few percent. The partially ascending slopes for few data points in dependence of the excitation wavelength is assigned to superimposed PL. The mode energies are directly compared to the calculated joint density of states (jDOS) of the individual transitions displayed in Fig. S1(c) in dependence of the position of E_F (color code) demonstrating its significant E_F -dependency. Mode energies and the jDOS are in good quantitative agreement assuming a realistic Fermi-energy of less than a few meV. In the energy range between 50 meV and 80 meV two well separated modes can be identified that are assigned to two $m_1 \rightarrow m_3$ and one $m_1 \rightarrow m_4$ transitions, the third one might be another $m_1 \rightarrow m_3$ superimposed by PL. The mode observed at an energy of about 95 meV is assigned to $m_1 \rightarrow m_5$ transition and the modes observed around 123 meV and 140 meV to $m_1 \rightarrow m_6$ and $m_1 \rightarrow m_7$ and higher transitions, respectively. Minor deviation between theory and experiment can have following concurrent origins: (i) The moiré bands are flat but still dispersing in a highly non-parabolic manner such that they themselves have a finite width of up to few tens of meV with overlapping bands particularly for m_3 and higher. (ii) Non-vertical transitions between points with a high DOS are expected to

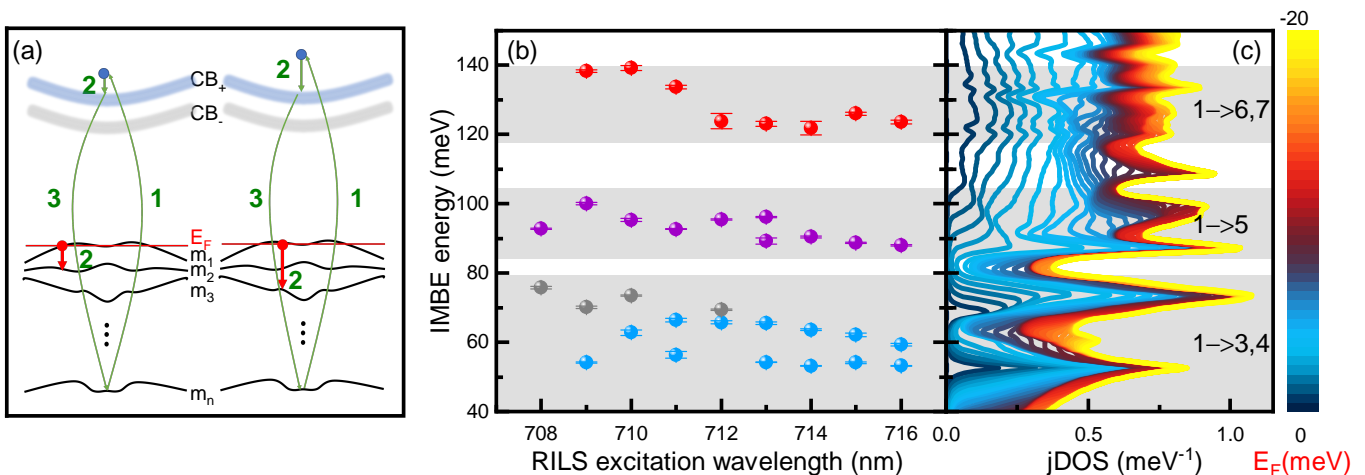


FIG. 2. (a) Schematic picture of the three-step scattering process for creation of IMBE between moiré minibands formed in the VB around the K points. In the first step an electron is excited from a lower VB to a virtual state; in the second step the charge carrier is scattered by Coulomb interaction with photo-excited hole from m_1 to m_2 (left) and from m_1 to m_3 (right) under creation of an IMBE. In the third step the electron recombines. (b) Extracted peak energies from the line-shape analysis described in Fig. 1 for 3° tWSe₂. (c) Calculated joint density of states jDOS for inter-miniband transitions in dependence of the Fermi-level E_F (color coded) of 3° tWSe₂ for vertical transitions. The peaks of the theoretical jDOS calculation are in good agreement with the Lorentzian fits to the experimental data (b).

contribute to finite momentum transfer q_{\parallel} in addition to defect induced breakdown of momentum conservation [40]. (iii) Twist angle variations of at least $\pm 0.3^\circ$ within the laser spot has a crucial impact on the moiré bands formation as discussed below.

In Fig. 3, we contrast RILS spectra in a false color representation taken on 3° tWSe₂ (a), natural bilayer (NBL) WSe₂ (b) and 8° tWSe₂ (c) for an extended range of excitation wavelengths. RILS intensities are encoded in the color scheme. In the RILS spectra of the twisted bilayers 3° tWSe₂ and 8° tWSe₂ displayed in Figs. 3(a) and (c), highly resonant, intense and rather broad RILS modes interpreted as IMBE dominate the RILS spectra. In addition to the phonon and IMBE resonances, a few features occur with energies depending on the incoming laser energy (tiled cyan lines) that are interpreted as defect or 0D-moiré potential localized emission signatures. The double resonance behaviour with a splitting of 15 meV only observed for 3° is in agreement with reported splitting in absorption and emission spectra for lower twist angles [21].

For the NBL sample despite the sharp phonon resonance, no clear RILS modes occur. The spectra are dominated by typical emission signatures. These lines are likely due to emission from interlayer excitons [19]. The absence of RILS modes for NBL is expected due to the absence of moiré lattice and minibands. The energy separation of the SOI-split valence bands is in the order of a few hundreds of meV [41] and hence far beyond the investigated energy range. For the 8° tWSe₂, instead, one weaker and one dominant broad RILS res-

onance appear at an energy range of about 60 meV to 120 meV. In this energy range, a good fit to the RILS spectra is achieved by a sum of two-Lorentzian terms [see example spectrum with fit overlaid in Fig. 3(c)]. For a quantitative comparison with theory, the related band structure for the moiré mBZ around the VBM at the K-point is displayed in Fig. 3(d) in the experimentally relevant energy range (for extended range see SI-Fig. 7 [32]). For such a large twist, the bands are nearly parabolic with larger energy separation. In comparison with theory, the weaker RILS mode at ≈ 60 meV could be interpreted as a collective intraband transition within the m_1 -band as sketched in Fig. 3(d). The more intense, broader RILS mode at $\approx 75 - 115$ meV is interpreted as an IMBE $m_1 \rightarrow m_2$ transition with the broadening due to non-vertical transitions provided by the finite transferred in-plane momentum $q_{\parallel} \leq q_{\max}$. The good quantitative agreement justifies our interpretation of the modes as being collective intra- and interband excitations allowing to study the band-structure of the mBZ at the K-points. In the following, we consider the impact of realistic twist-angle variations to be in the order of $\pm 0.3^\circ$. While it is shown from calculated bands to be negligible small for $(8 \pm 0.5)^\circ$ tWSe₂, the impact is significant in the miniband energies and dispersion for $(3 \pm 0.3)^\circ$ tWSe₂ as plotted in Fig. 3(e). As highlighted above, twist angle variation together with non-vertical transitions and finite momentum transfer results in broadened IMBE signatures in RILS. The RILS modes are a convolution of jDOS and the momentum distribution. We would like to note that we do not observe sizeable differences for linear-co

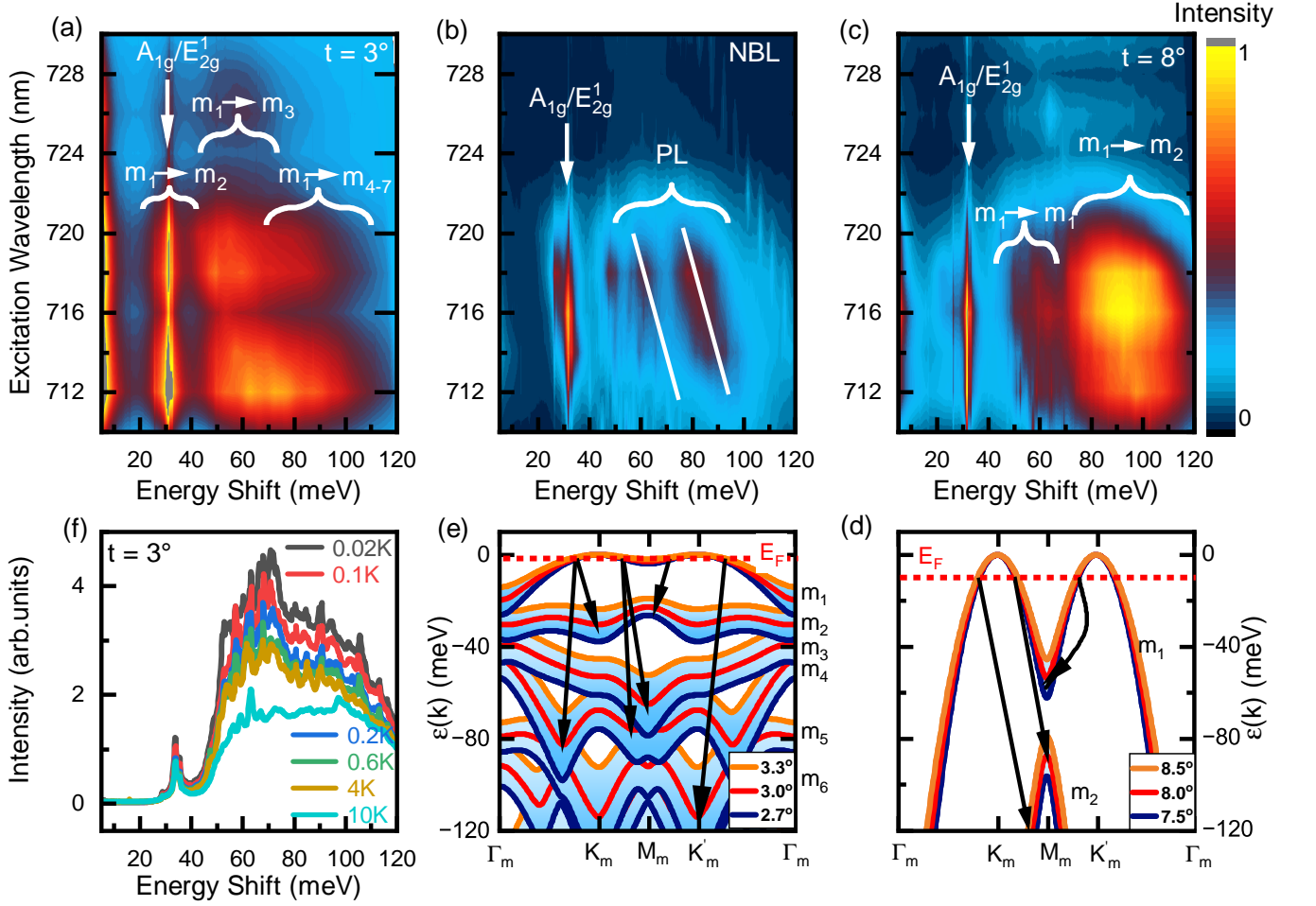


FIG. 3. RILS spectra on (a) 3° tWSe₂, (b) natural bilayer (NBL) and (c) WSe₂ 8° tWSe₂. The straight white arrows indicate phonon modes and the white curly braces in (a) and (c) IMBE with moiré band assignment according to calculations. In the natural bilayer spectra (b) in addition to the vertical phonon line only shifting emission signals marked with tilted white lines emerge. In (c) an individual spectrum is exemplarily overlaid in grey color with a fit to the data (blue line) using the sum of two Lorentz curves. [$T = 4\text{K}$, $P_{\text{laser}} = 500\mu\text{W}$; inset: $\lambda_{\text{laser}} = 712\text{nm}$]. (d) Calculated electronic band structure for $(8^\circ \pm 0.5^\circ)$ considering realistic twist variations. (e) Calculated electronic band structure for $(3^\circ \pm 0.3^\circ)$. Twist variations can result in broadened minibands causing significantly broadened IMBE in RILS experiments. Breakdown of wave-vector conservation together with finite transferred in-plane momentum q_{\parallel} due to the high NA of the objective allows also for non-vertical to points of the minibands with high DOS as indicated by the arrows. (f) Temperature dependent RILS spectra for $10\text{mK} < T < 10\text{K}$ for 3° tWSe₂. [$\lambda_{\text{exc}} = 710\text{nm}$, $P_{\text{laser}} = 50\mu\text{W}$]. RILS signals fade out with increasing temperature and at 10K only a weak signal superimposed by emission background remains.

and linear-cross polarization in the RILS spectra (see SI-Fig.6 [32]). This finding supports our interpretation that the RILS modes are single-particle type of IMBE rather than plasma-like charge-density or spin-density excitations that show both a distinct polarization dependence [34]. To further substantiate our interpretation, we perform temperature dependent RILS measurements (Fig. 3(f)). To avoid heating effects, the excitation power is reduced to $P = 50\mu\text{W}$ and the excitation wavelength kept constant at extreme resonance condition at $\lambda = 710\text{nm}$. The RILS signal shows a clear temperature dependence and is reduced with increasing temperature. Already at 10K the RILS modes fade out and the PL background

starts to dominate the spectrum. We observe similar reduction in RILS intensity with increasing temperature for the 8° tWSe₂ sample (see SI-Fig.6 [32]). All experimental observations together strongly support the interpretation that the observed broad RILS signatures are indeed collective IMBE between moiré bands at the VBM at the K/K' valley in excellent agreement to theory. We would like to emphasize that collective excitations probe the weakly disordered parts of the sample, while disorder often results in the most dominant signatures in emission experiments due to rather bright localized emission and disturbs transport investigations by additional scattering channels.

To conclude, we establish that low-temperature RILS experiments on collective "single particle like" [29, 31, 34] IMBE on twisted WSe₂ bilayers is a powerful method to experimentally study the moiré band formation selectively at the VBM around the K/K' states, their energetic separation and twist angle dependence providing a promising approach to study the band structure of twisted TMDCs at twist angles where correlation physics play an important role [4, 12, 13, 16–18]. In agreement with theory, we identify several IMBE for a 3° tWSe₂, while for a 8° tWSe₂ only one clear IMBE and presumably one collective intraband excitation is observable and none natural bilayers. The observation of collective IMBE by RILS in a semiconducting vdW bilayer demonstrates the potential to access the collective low-lying excitation spectra as unique fingerprints of individual quantum phases by RILS similar to correlated phases e.g. in the fractional quantum Hall effect regime [42–44].

The authors gratefully acknowledge the German Science Foundation (DFG) for financial support via Grants WU 637/7-1, WE 5342/5-1 and the Priority Program SPP 2244 "2DMP" - 443273985, 443274199 as well as the computing time granted through JARA on the supercomputer JURECA [45] at Forschungszentrum Jülich. LK acknowledges support from the DFG through FOR 5249 (QUAST, Project No. 449872909). TW acknowledges support by the Cluster of Excellence 'CUI: Advanced Imaging of Matter' of the DFG (EXC 2056, Project ID 390715994). DMK acknowledges support by the Deutsche Forschungsgemeinschaft (DFG, German Research Foundation) under Germany's Excellence Strategy - Cluster of Excellence Matter and Light for Quantum Computing (ML4Q) EXC 2004/1 - 390534769. We acknowledge support by the Max Planck-New York City Center for Nonequilibrium Quantum Phenomena.

-
- [1] D. M. Kennes, M. Claassen, L. Xian, A. Georges, A. J. Millis, J. Hone, C. R. Dean, D. N. Basov, A. N. Pasupathy, and A. Rubio, Moiré heterostructures as a condensed-matter quantum simulator, *Nature Physics* **17**, 155 (2021).
- [2] Y. Tang, L. Li, T. Li, Y. Xu, S. Liu, K. Barmak, K. Watanabe, T. Taniguchi, A. H. MacDonald, J. Shan, and K. F. Mak, Simulation of hubbard model physics in wse2/ws2 moiré superlattices, *Nature* **579**, 353 (2020).
- [4] F. Wu, T. Lovorn, E. Tutuc, and A. H. MacDonald, Hubbard Model Physics in Transition Metal Dichalcogenide Moiré Bands, *Physical Review Letters* **121**, 026402 (2018).
- [4] L. Balents, C. R. Dean, D. K. Efetov, and A. F. Young, Superconductivity and strong correlations in moiré flat bands, *Nature Physics*, 1 (2020).
- [5] P. A. Pantaleón, A. Jimeno-Pozo, H. Sainz-Cruz, V. T. Phong, T. Cea, and F. Guinea, Superconductivity and correlated phases in non-twisted bilayer and trilayer graphene, *Nat Rev Phys* **5**, 304 (2023).
- [6] Y. Cao, V. Fatemi, S. Fang, K. Watanabe, T. Taniguchi, E. Kaxiras, and P. Jarillo-Herrero, Unconventional superconductivity in magic-angle graphene superlattices, *Nature* **556**, 43 (2018).
- [7] Y. Cao, V. Fatemi, A. Demir, S. Fang, S. L. Tomarken, J. Y. Luo, J. D. Sanchez-Yamagishi, K. Watanabe, T. Taniguchi, E. Kaxiras, R. C. Ashoori, and P. Jarillo-Herrero, Correlated insulator behaviour at half-filling in magic-angle graphene superlattices, *Nature* **556**, 80 (2018).
- [8] Z. Hao, A. M. Zimmerman, P. Ledwith, E. Khalaf, D. H. Najafabadi, K. Watanabe, T. Taniguchi, A. Vishwanath, and P. Kim, Electric field-tunable superconductivity in alternating-twist magic-angle trilayer graphene, *Science* **371**, 1133 (2021).
- [9] J. M. Park, Y. Cao, K. Watanabe, T. Taniguchi, and P. Jarillo-Herrero, Tunable strongly coupled superconductivity in magic-angle twisted trilayer graphene, *Nature* **590**, 249 (2021).
- [10] Y. Zhang, R. Polski, C. Lewandowski, A. Thomson, Y. Peng, Y. Choi, H. Kim, K. Watanabe, T. Taniguchi, J. Alicea, F. von Oppen, G. Refael, and S. Nadj-Perge, Promotion of superconductivity in magic-angle graphene multilayers, *Science* **377**, 1538 (2022).
- [11] F. Wu, T. Lovorn, E. Tutuc, I. Martin, and A. H. MacDonald, Topological insulators in twisted transition metal dichalcogenide homobilayers, *Phys. Rev. Lett.* **122**, 086402 (2019).
- [12] J. Zang, J. Wang, J. Cano, and A. J. Millis, Hartree-fock study of the moiré hubbard model for twisted bilayer transition metal dichalcogenides, *Phys. Rev. B* **104**, 075150 (2021).
- [13] L. Xian, M. Claassen, D. Kiese, M. M. Scherer, S. Trebst, D. M. Kennes, and A. Rubio, Realization of nearly dispersionless bands with strong orbital anisotropy from destructive interference in twisted bilayer mos2, *Nature Communications* **12**, 5644 (2021).
- [14] L. Wang, E.-M. Shih, A. Ghiotto, L. Xian, D. A. Rhodes, C. Tan, M. Claassen, D. M. Kennes, Y. Bai, B. Kim, K. Watanabe, T. Taniguchi, X. Zhu, J. Hone, A. Rubio, A. N. Pasupathy, and C. R. Dean, Correlated electronic phases in twisted bilayer transition metal dichalcogenides, *Nature Materials* **19**, 861 (2020).
- [15] A. Ghiotto, E.-M. Shih, G. S. S. G. Pereira, D. A. Rhodes, B. Kim, J. Zang, A. J. Millis, K. Watanabe, T. Taniguchi, J. C. Hone, L. Wang, C. R. Dean, and A. N. Pasupathy, Quantum criticality in twisted transition metal dichalcogenides, *Nature* **597**, 345 (2021).
- [16] S. Rye and T. O. Wehling, Switching between mott-hubbard and hund physics in moiré quantum simulators, *Nano Letters* **23**, 573 (2023).
- [17] L. Klebl, A. Fischer, L. Classen, M. M. Scherer, and D. M. Kennes, Competition of density waves and superconductivity in twisted tungsten diselenide, *Phys. Rev. Res.* **5**, L012034 (2023).
- [18] Y.-M. Wu, Z. Wu, and H. Yao, Pair-Density-Wave and Chiral Superconductivity in Twisted Bilayer Transition Metal Dichalcogenides, *Phys. Rev. Lett.* **130**, 126001 (2023).
- [19] Z. Wang, Y.-H. Chiu, K. Honz, K. F. Mak, and J. Shan, Electrical tuning of interlayer exciton gases in wse2 bilayers, *Nano Letters* **18**, 137 (2018), pMID: 29240440.
- [20] D. Halbertal, N. R. Finney, S. S. Sunku, A. Kerelsky, C. Rubio-Verdú, S. Shabani, L. Xian, S. Carr, S. Chen,

- C. Zhang, L. Wang, D. Gonzalez-Acevedo, A. S. McLeod, D. Rhodes, K. Watanabe, T. Taniguchi, E. Kaxiras, C. R. Dean, J. C. Hone, A. N. Pasupathy, D. M. Kennes, A. Rubio, and D. N. Basov, Moiré metrology of energy landscapes in van der waals heterostructures, *Nature Communications* **12**, 242 (2021).
- [21] T. I. Andersen, G. Scuri, A. Sushko, K. De Greve, J. Sung, Y. Zhou, D. S. Wild, R. J. Gelly, H. Heo, D. Bérubé, A. Y. Joe, L. A. Jauregui, K. Watanabe, T. Taniguchi, P. Kim, H. Park, and M. D. Lukin, Excitons in a reconstructed moiré potential in twisted WSe₂/WSe₂ homobilayers, *Nature Materials* **20**, 480 (2021).
- [22] E. Li, J.-X. Hu, X. Feng, Z. Zhou, L. An, K. T. Law, N. Wang, and N. Lin, Lattice reconstruction induced multiple ultra-flat bands in twisted bilayer WSe₂, *Nature Communications* **12**, 5601 (2021).
- [23] S. Zhao, Z. Li, X. Huang, A. Rupp, J. Göser, I. A. Vovk, S. Y. Kruchinin, K. Watanabe, T. Taniguchi, I. Bilgin, A. S. Baimuratov, and A. Högele, Excitons in mesoscopically reconstructed moiré heterostructures, *Nature Nanotechnology* 10.1038/s41565-023-01356-9 (2023).
- [24] M. Troue, J. Figueiredo, L. Sigl, C. Paspalides, M. Katzer, T. Taniguchi, K. Watanabe, M. Selig, A. Knorr, U. Wurstbauer, and A. W. Holleitner, Extended spatial coherence of interlayer excitons in mose₂/wse₂ heterobilayers, *Phys. Rev. Lett.* **131**, 036902 (2023).
- [25] O. Karni, E. Barré, V. Pareek, J. D. Georganas, M. K. L. Man, C. Sahoo, D. R. Bacon, X. Zhu, H. B. Ribeiro, A. L. O’Beirne, J. Hu, A. Al-Mahboob, M. M. M. Abdelrasoul, N. S. Chan, A. Karmakar, A. J. Winchester, B. Kim, K. Watanabe, T. Taniguchi, K. Barmak, J. Madéo, F. H. da Jornada, T. F. Heinz, and K. M. Dani, Structure of the moiré exciton captured by imaging its electron and hole, *Nature* **603**, 247 (2022).
- [26] A. Sood, J. B. Haber, J. Carlström, E. A. Peterson, E. Barre, J. D. Georganas, A. H. M. Reid, X. Shen, M. E. Zajac, E. C. Regan, J. Yang, T. Taniguchi, K. Watanabe, F. Wang, X. Wang, J. B. Neaton, T. F. Heinz, A. M. Lindenberg, F. H. da Jornada, and A. Raja, Bidirectional phonon emission in two-dimensional heterostructures triggered by ultrafast charge transfer, *Nature Nanotechnology* **18**, 29 (2023).
- [27] Z. Zhang, Y. Wang, K. Watanabe, T. Taniguchi, K. Ueno, E. Tutuc, and B. J. LeRoy, Flat bands in twisted bilayer transition metal dichalcogenides, *Nature Physics* **16**, 1093 (2020).
- [28] G. Gatti, J. Issing, L. Rademaker, F. Margot, T. A. de Jong, S. J. van der Molen, J. Teyssier, T. K. Kim, M. D. Watson, C. Cacho, P. Dudin, J. Avila, K. C. Edwards, P. Paruch, N. Ubrig, I. Gutiérrez-Lezama, A. F. Morpurgo, A. Tamai, and F. Baumberger, Flat Γ moiré bands in twisted bilayer wse₂, *Phys. Rev. Lett.* **131**, 046401 (2023).
- [29] A. Pinczuk, L. Brillson, E. Burstein, and E. Anastassakis, Resonant light scattering by single-particle electronic excitations in n -GaAs, *Phys. Rev. Lett.* **27**, 317 (1971).
- [30] G. Abstreiter, T. Egeler, S. Beeck, A. Seilmeier, H. Hübner, G. Weimann, and W. Schlapp, Electronic excitations in narrow gaas/algaas quantum well structures, *Surface Science* **196**, 613 (1988).
- [31] S. Das Sarma and D.-W. Wang, Resonant raman scattering by elementary electronic excitations in semiconductor structures, *Phys. Rev. Lett.* **83**, 816 (1999).
- [32] See supplemental material [url] which includes refs. [46-48].
- [33] G. Abstreiter and K. Ploog, Inelastic light scattering from a quasi-two-dimensional electron system in gaas-al_xga_{1-x}As heterojunctions, *Phys. Rev. Lett.* **42**, 1308 (1979).
- [34] S. Meier, P. E. F. Junior, F. Haas, E.-S. Heller, F. Dirnberger, V. Zeller, T. Korn, J. Fabian, D. Bougeard, and C. Schüller, Intersubband excitations in ultrathin core-shell nanowires in the one-dimensional quantum limit probed by resonant inelastic light scattering, *Phys. Rev. B* **104**, 235307 (2021).
- [8] L. P. McDonnell, J. J. S. Viner, P. Rivera, X. Xu, and D. C. Smith, Observation of intravalley phonon scattering of 2s excitons in mose₂ and wse₂ monolayers, *2D Materials* **7**, 045008 (2020).
- [5] H. Pan, F. Wu, and S. Das Sarma, Band topology, Hubbard model, Heisenberg model, and Dzyaloshinskii-Moriya interaction in twisted bilayer $\{\mathrm{WSe}\}_2$, *Physical Review Research* **2**, 033087 (2020).
- [6] T. Devakul, V. Crépel, Y. Zhang, and L. Fu, Magic in twisted transition metal dichalcogenide bilayers, *Nature Communications* **12**, 6730 (2021).
- [7] S. Ryee and T. O. Wehling, Switching between Mott-Hubbard and Hund Physics in Moiré Quantum Simulators, *Nano Letters* **23**, 573 (2023).
- [39] S. Brem, K.-Q. Lin, R. Gillen, J. M. Bauer, J. Maultzsch, J. M. Lupton, and E. Malic, Hybridized intervalley moiré excitons and flat bands in twisted wse₂ bilayers, *Nanoscale* **12**, 11088 (2020).
- [40] U. Wurstbauer, D. Majumder, S. S. Mandal, I. Dujovne, T. D. Rhone, B. S. Dennis, A. F. Rigosi, J. K. Jain, A. Pinczuk, K. W. West, and L. N. Pfeiffer, Observation of nonconventional spin waves in composite-fermion ferromagnets, *Phys. Rev. Lett.* **107**, 066804 (2011).
- [41] A. Kormányos, G. Burkard, M. Gmitra, J. Fabian, V. Zólyomi, N. D. Drummond, and V. Fal’ko, Corrigendum: k.p theory for two-dimensional transition metal dichalcogenide semiconductors (2015 2d mater. 2 022001), *2D Materials* **2**, 049501 (2015).
- [42] U. Wurstbauer, K. W. West, L. N. Pfeiffer, and A. Pinczuk, Resonant inelastic light scattering investigation of low-lying gapped excitations in the quantum fluid at $\nu=5/2$, *Phys. Rev. Lett.* **110**, 026801 (2013).
- [43] L. Du, U. Wurstbauer, K. W. West, L. N. Pfeiffer, S. Fallahi, G. C. Gardner, M. J. Manfra, and A. Pinczuk, Observation of new plasmons in the fractional quantum hall effect: Interplay of topological and nematic orders, *Science Advances* **5**, eaav3407 (2019).
- [44] J. Liang, Z. Liu, Z. Yang, Y. Huang, U. Wurstbauer, C. R. Dean, K. W. West, L. N. Pfeiffer, L. Du, and A. Pinczuk, Evidence for chiral graviton modes in fractional quantum hall liquids, *Nature* 10.1038/s41586-024-07201-w (2024).
- [45] Jülich Supercomputing Centre, JURECA: Data Centric and Booster Modules implementing the Modular Supercomputing Architecture at Jülich Supercomputing Centre, *Journal of large-scale research facilities* **7**, 10.17815/jlsrf-7-182 (2021).
- [1] G. Scuri, T. I. Andersen, Y. Zhou, D. S. Wild, J. Sung, R. J. Gelly, D. Bérubé, H. Heo, L. Shao, A. Y. Joe, A. M. Mier Valdivia, T. Taniguchi, K. Watanabe, M. Lončar, P. Kim, M. D. Lukin, and H. Park, Electrically tunable valley dynamics in twisted wse₂/wse₂ bilayers, *Phys. Rev. Lett.* **124**, 217403 (2020).

- [2] F. Sigger, H. Lambers, K. Nisi, J. Klein, N. Sai-
gal, A. W. Holleitner, and U. Wurstbauer, Spec-
troscopic imaging ellipsometry of two-dimensional
TMDC heterostructures, *Applied Physics Letters*
121, 071102 (2022), [https://pubs.aip.org/aip/apl/article-
pdf/doi/10.1063/5.0109189/16481539/071102_1_online.pdf](https://pubs.aip.org/aip/apl/article-pdf/doi/10.1063/5.0109189/16481539/071102_1_online.pdf).
- [3] J. P. Bange, P. Werner, D. Schmitt, W. Bennecke,
G. Meneghini, A. AlMutairi, M. Merboldt, K. Watanabe,
T. Taniguchi, S. Steil, D. Steil, R. T. Weitz, S. Hofmann,
G. S. M. Jansen, S. Brem, E. Malic, M. Reutzler, and
S. Mathias, Ultrafast dynamics of bright and dark exci-
tons in monolayer wse2 and heterobilayer wse2/mos2, *2D*
Materials **10**, 035039 (2023)

Supplemental Materials: Collective charge excitations between moiré-minibands in twisted WSe₂ bilayers from resonant inelastic light scattering

METHODS AND EXPERIMENTAL PROCEDURE

Sample preparation

The tWSe₂ samples were prepared by first mechanically exfoliating the monolayer WSe₂ and multilayer hBN crystals onto viscoelastic PDMS stamps followed by their deterministic dry transfer (DDT) using a home-built setup with x-y-z and rotational micro-manipulators. To fix the stacking (twist) angle between the WSe₂ monolayers, their crystalline edges were determined from optical images on the PDMS stamps. Following this, the top WSe₂ monolayer was stacked on top of the bottom WSe₂ monolayer at the desired twist angle by using a rotation stage attached to the sample stage in the DDT setup. After preparation of the full heterostructure including the hBN encapsulation layers, the samples were annealed in a home-built vacuum annealing chamber at a nominal pressure in the order of 5×10^{-5} mbar at 100 - 120 °C for 5 - 6 hours. An optical micrograph of a prepared 3° tWSe₂ sample as an example is shown in the inset of SI-Fig.1.

Photoluminescence (PL) and non-resonant Raman spectroscopy

After preparation of the samples, they were characterized by low temperature non-resonant PL and Raman spectroscopies. The samples were mounted on the cold finger equipped with x-y-z piezo stages of a dilution refrigerator. The samples were cooled down to 4K using pulse tube refrigeration operating with helium gas. For non-resonant characterization measurements, a 532 nm (2.33 eV) solid state laser, cleaned up using a grating based monochromator with a 1nm bandpass, was used for excitation of the samples. The laser was focused on the samples with a low temperature compatible objective lens with an NA of 0.82 mounted on a homebuilt stage attached to the 4K cryoshield of the refrigerator. The focused spot on the sample had a diameter of $\sim 2\mu\text{m}$. The emission and scattering signals from the sample were collected by the same objective lens in a back scattering geometry and dispersed using a single spectrometer with a 600 l/mm grating for PL and an 1800 l/mm grating for Raman spectroscopy. The focal length of the spectrometer was 750 mm and the spectral resolution (532 nm, 1800 l/mm grating) was $\sim 0.4 \text{ cm}^{-1}$. The Rayleigh scattered light was filtered out by using a 532 nm long pass filter in front of the spectrometer. The dispersed light was collected and measured using a liquid nitrogen cooled CCD camera. Position and laser power dependent PL and position dependent Raman measurements were used to select the region of the sample for subsequent resonant inelastic light scattering measurements.

Resonant Inelastic Light Scattering spectroscopy

Following the characterization by low temperature PL and Raman spectroscopy, inelastic light scattering spectra under resonant excitation conditions were measured. The samples were mounted inside a dilution refrigerator as described above. The samples were excited at energies between 1.698 eV (730 nm) and 1.771 eV (700 nm) using a continuously frequency tunable Ti:sapphire laser stabilized by a ring cavity with a linewidth of about 50kHz. The luminescence background from the Ti:sapphire crystal was removed by passing the excitation laser beam through a monochromator (1nm bandpass). The light emitted or scattered from the sample surface were again collected in back scattering geometry and sent to either a single spectrometer with a 600 l/mm grating or to a triple spectrometer with a grating combination of 300 l/mm, 300 l/mm and 600 l/mm. The triple spectrometer was used in a subtractive mode where the second stage of the spectrometer is used to suppress the dispersion generated by the first stage by appropriate alignment of the gratings. This meant that at the exit slit of the second stage, light could be filtered out based on the angle of entrance in the spectrometer. Thus, the first two stages served as a bandpass filter and filtered out any stray light not following the path of light scattered from the sample, as well as the Rayleigh scattered background.

Determination of photo-excited hole density in power-dependent measurements

For the estimation of the change in the photo-generated charge carrier density by excitation power dependent measurements, we start considering the generation rate of photo-generated electron-hole pairs given by:

$$G = \frac{P\sigma}{Ah\nu}, \quad (\text{S1})$$

where P is the power of the incident light in units Watt, σ is the absorbance of the sample at the specific excitation wavelength, A is the area of the sample in unit cm^{-2} and $h\nu$ is the energy of the photon in unit Joule. In the current experiment the excitation is done in continuous wave (cw) mode such that we can assume steady state conditions. The change in the photo-generated charge carries constitutes

$$\frac{dp}{dt} = G - \frac{p}{\tau} = 0 \quad (\text{S2})$$

and thus,

$$p = G\tau = \frac{P\sigma\tau}{Ah\nu} \quad (\text{S3})$$

with τ the lifetime of the photo-excited charge carriers reported to be $\approx 100\text{ps} - 1\text{ns}$ [S1]. We approximate the spot area of the sample by $A \approx 6\text{m}^2$. The optical absorbance of the $\text{WSe}_2/\text{MoSe}_2$ heterostructure in the relevant range of excitation wavelength of 700nm to 716nm ($1.73 - 1.77$ eV) is taken from spectroscopic imaging ellipsometry investigations [S2]. We would like to note that the carrier generation rate, the absorbance as well as lifetime can be subject of the change of carrier density itself. Following this approach, we approximate the change of the photogenerated charge carrier density, i.e. change in the hole density Δp in dependence of the excitation power as following:

- $P_{\text{Laser}} = 1\mu\text{W} \rightarrow \Delta p \approx 10^9\text{cm}^{-2}$,
- $P_{\text{Laser}} = 50\mu\text{W} \rightarrow \Delta p \approx 10^{10}\text{cm}^{-2}$,
- $P_{\text{Laser}} = 1\text{mW} \rightarrow \Delta p \approx 10^{12}\text{cm}^{-2}$.

We would like to note that the as exfoliated WSe_2 is typically slightly p-type doped. We assume the photo-generated holes for monolayers and also for the $t\text{WSe}_2$ bilayer to reside at the K, K'valley forming an two-dimensional hole gas with a quasi-Fermi level under steady state conditions. Particularly for the bilayer the situation is expected to be different for the conduction band. The Σ -valley is energetically lower compared to the K-valley such that efficient charge carrier relaxation to the Σ -valley is expected [S3]. As a direct consequence, an electron gas is expected to be formed rather at the Σ -valley compared to the K-valley. Therefore, at the K-valley probed in the RILS experiment in this study by the selected resonance conditions, an excess of holes is assumed such that the RILS experiment is sensitive to the collective excitation of the two-dimensional hole plasma formed at the VB top at the K valley around which the moiré minibands are formed.

THEORETICAL CALCULATIONS

Continuum Hamiltonian

In the small-angle approximation $\Theta \sim 0^\circ$, the dispersion of $t\text{WSe}_2$ can be obtained by constructing a continuum model (following Refs. [S4–S7]). As the electrons in a WSe_2 monolayer are spin-valley locked, only one valley per layer contributes to each spin sector of the moiré Hamiltonian

$$H_{\uparrow}(\mathbf{k}) = \begin{pmatrix} -\frac{\hbar^2(\mathbf{k}-K_1)^2}{2m^*} + \Delta_1(\mathbf{r}) & \Delta_T(\mathbf{r}) \\ \Delta_T^\dagger(\mathbf{r}) & -\frac{\hbar^2(\mathbf{k}-K_2)^2}{2m^*} + \Delta_2(\mathbf{r}) \end{pmatrix}, \quad (\text{S4})$$

where $m^* = 0.43 m_e$ is the effective mass, K_l the original K -point of layer $l = 1, 2$, $\Delta_T(\mathbf{r})$ the interlayer potential, and $\Delta_l(\mathbf{r})$ the intralayer potential. The other spin sector $H_{\downarrow}(\mathbf{k})$ is obtained from time reversal symmetry. The inter- and intralayer potentials are parameterized by the following simple formulæ:

$$\Delta_l(\mathbf{r}) = 2V \sum_{\mathbf{g} \in \Delta} \cos(\mathbf{g} \cdot \mathbf{r} + \sigma_z^l \psi), \quad \Delta_T(\mathbf{r}) = w \sum_{\mathbf{g} \in \Delta} e^{-i\mathbf{g} \cdot \mathbf{r}}. \quad (\text{S5})$$

Here, σ_z is the Pauli z matrix and \mathbf{g} are three reciprocal moiré lattice vectors that are connected by C_3 rotations. Hence we index the summation over those three reciprocal moiré lattice vectors as $\mathbf{g} \in \Delta$. The K - and K' -points in the moiré Brillouin zone (BZ) coincide with K_1 and K_2 , respectively.

The intralayer potential strength $V = 9$ meV, the interlayer hopping $w = 18$ meV, and the intralayer potential parameter $\psi = 128^\circ$ are taken to match density functional theory results [S6]. Note that the twist angle Θ enters Eq. (S4) through geometry in the momentum argument \mathbf{k} as well as the length of the inverse moiré lattice vectors \mathbf{g} in Eq. (S5).

For numerical diagonalization of the Hamiltonian Eq. (S4), the expansion in inverse moiré lattice vectors must be truncated. We take into account the following inverse moiré lattice vectors \mathbf{G}

$$\mathbf{G} \in \{\mathbf{H} \mid \|\mathbf{H}\| \leq 3\|\mathbf{g}\| \ \forall \mathbf{g} \in \Delta\}, \quad (\text{S6})$$

i.e., a distance shell cutoff with length 3, which is sufficient for convergence of the resulting band structures.

Joint Density of States

The joint density of states (jDOS) data in Fig. 3 (f) of the main text is obtained numerically from the model discussed above. In essence, we implement the following formula:

$$\text{jDOS}(\omega) = \text{Im} \frac{1}{N_{\mathbf{k}}} \sum_{\mathbf{k}, b_1, b_2} \frac{f(\epsilon_{b_1}(\mathbf{k})) - f(\epsilon_{b_2}(\mathbf{k}))}{\omega - i\eta + \epsilon_{b_1}(\mathbf{k}) - \epsilon_{b_2}(\mathbf{k})}, \quad (\text{S7})$$

where $\epsilon_b(\mathbf{k})$ is the dispersion of band b with \mathbf{k} in the mini BZ, $f(x) = (1 + \exp[\beta(x - \mu)])^{-1}$ the Fermi function, and $\eta = 5$ meV a Lorentzian broadening. The inverse temperature is set to $\beta = 10^2$ meV $^{-1}$. As we perform massive scans in frequency ω and chemical potential μ (Fermi energy) for significant \mathbf{k} -meshes (96×96 regularly spaced points in the primitive zone), we make use of the parallel nature of Eq. (S7) using a custom GPU implementation.

ADDITIONAL FIGURES

Low-temperature photoluminescence spectrum of tWSe₂ ($t = 3$)

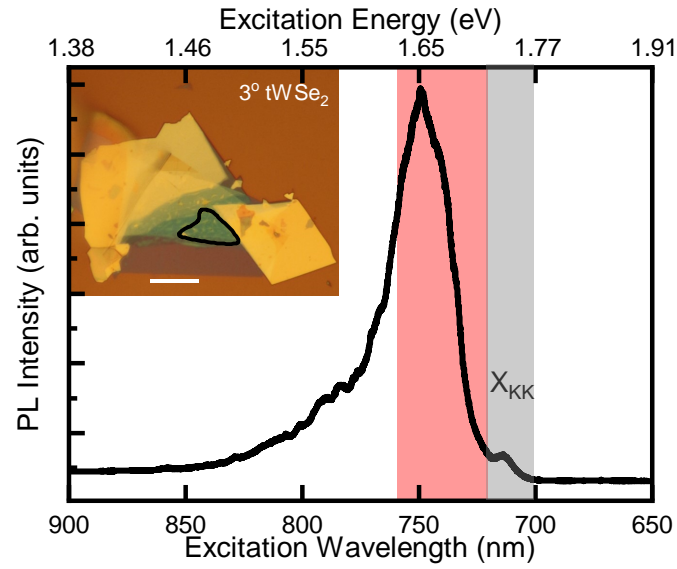


FIG. S1. (a) PL spectrum shows weak emission from direct K/K' excitons (X_{KK}) and a intense broad emission band from dark, charged and defect bound excitons. The spectral range around (X_{KK}) utilized for RILS spectroscopy is grey shaded and the region where modes in RILS are expected red shaded [$T = 4\text{K}$, $P_{\text{Laser}} = 1\text{mW}$, $E_{\text{Laser}} = 2.33\text{eV}$]. Inset: Optical micrograph of a hBN encapsulated 3° tWSe₂ sample with active region marked marked by black line. [scale bar 20 μm]

Non-resonant Raman measurements

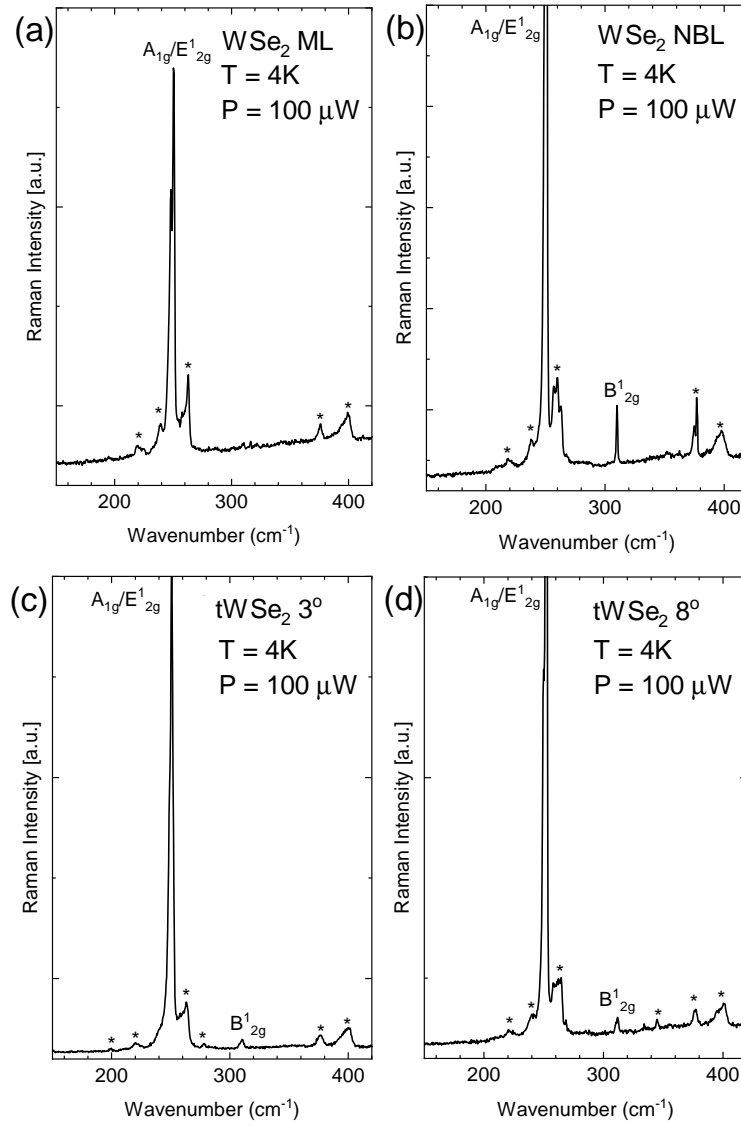


FIG. S2. (a) Non-resonant Raman spectra on hBN encapsulated WSe₂ monolayer, (b) hBN encapsulated natural bilayer (NBL) WSe₂, (c) hBN encapsulated 3° tWSe₂ and (c) hBN encapsulated 8° tWSe₂. All spectra show the optical phonon modes A_{1g}, E_{2g}¹ and in addition the NBL and twisted bilayers show the B_{2g}¹ phonon mode. The features marked by an asterisk (*) are due to multiphonon scattering processes [T = 4K, P_{laser} = 100 μW, E_{laser} = 2.33eV].

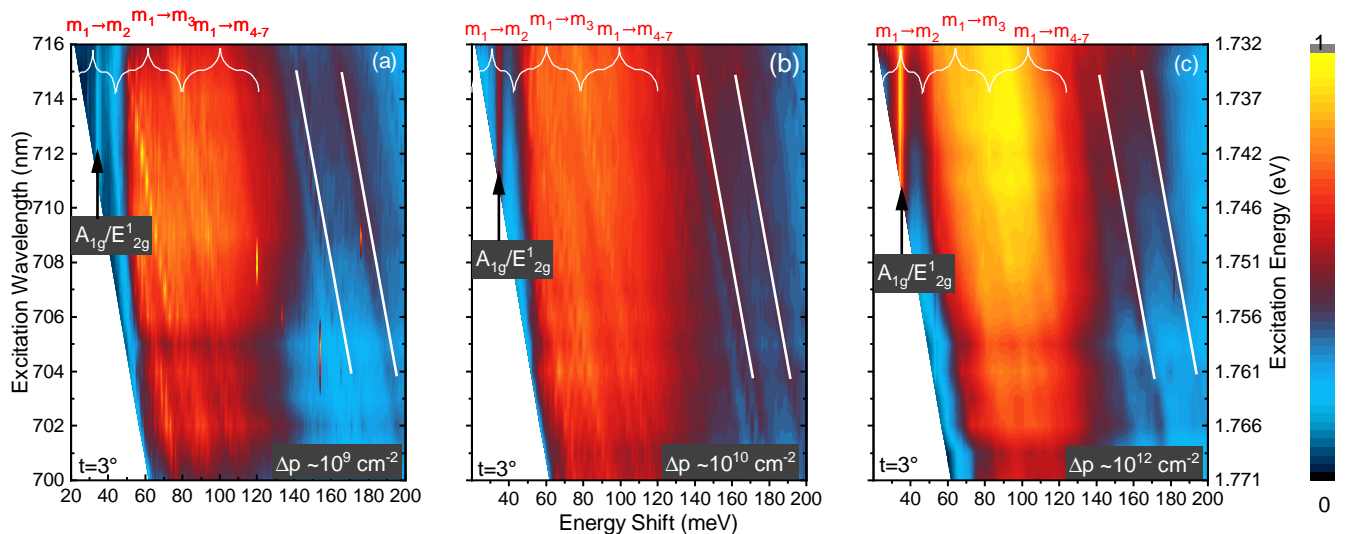
Excitation power dependent RILS measurements on $t\text{WSe}_2$ ($t = 3$)

FIG. S3. (a) False color plots of RILS spectra for 3° $t\text{WSe}_2$ at three different excitation powers of (a) $1\mu\text{W}$, (b) $50\mu\text{W}$ and (c) 1mW , respectively. The corresponding changes in the photo-excited hole-densities are $\sim 10^9\text{ cm}^{-2}$, $\sim 10^{10}\text{ cm}^{-2}$ and $\sim 10^{12}\text{ cm}^{-2}$, respectively. The phonon-lines are marked by straight arrows and emission features by tilted cyan solid lines. White braces indicate the energy positions of IMBE. Particularly the $m_1 \rightarrow m_2$ transition is enhanced with increasing doping and hence position of E_F in agreement with $\text{jDOS}(E_F)$ [$T = 4\text{K}$].

Excitation-power dependent RILS measurements are performed for the 3° $t\text{WSe}_2$ sample in order to vary E_F by the photo-induced holes. RILS spectra from a different set of experiments are compared in Fig. S3 for (a) $1\mu\text{W}$ corresponding to a change in the hole density by $\Delta p \approx 10^9\text{ cm}^{-2}$, (b) $50\mu\text{W}$ ($\Delta p \approx 10^{10}\text{ cm}^{-2}$) and (c) 1mW ($\Delta p \approx 10^{12}\text{ cm}^{-2}$), respectively.

Due to the strong band non-parabolicity and the unknown intrinsic doping it is not possible to estimate the change in E_F from δp . While it is not possible within the experimental certainty to clearly identify a shift in the energy, the intensity of the RILS mode assigned to IMBE $m_1 \rightarrow m_2$ is significantly reduced for the low density measurements as expected from the jDOS . Similarly, for the high energy transition that seems to be most pronounced for the higher power measurements indicated by an even broader overlapping emission band towards 100meV and beyond. This is most pronounced for $50\mu\text{W}$. For the 1mW spectra some spectral weight shifts back to the intermediate transitions regions $m_1 \rightarrow m_{4,5}$. This also agrees with the jDOS from the band structure calculation and strongly supports our interpretation that the observed broad RILS signatures are indeed collective IMBE between moiré bands at the VBM.

Lineshape-analysis of power dependent RILS data of $tWSe_2$ ($t = 3$)

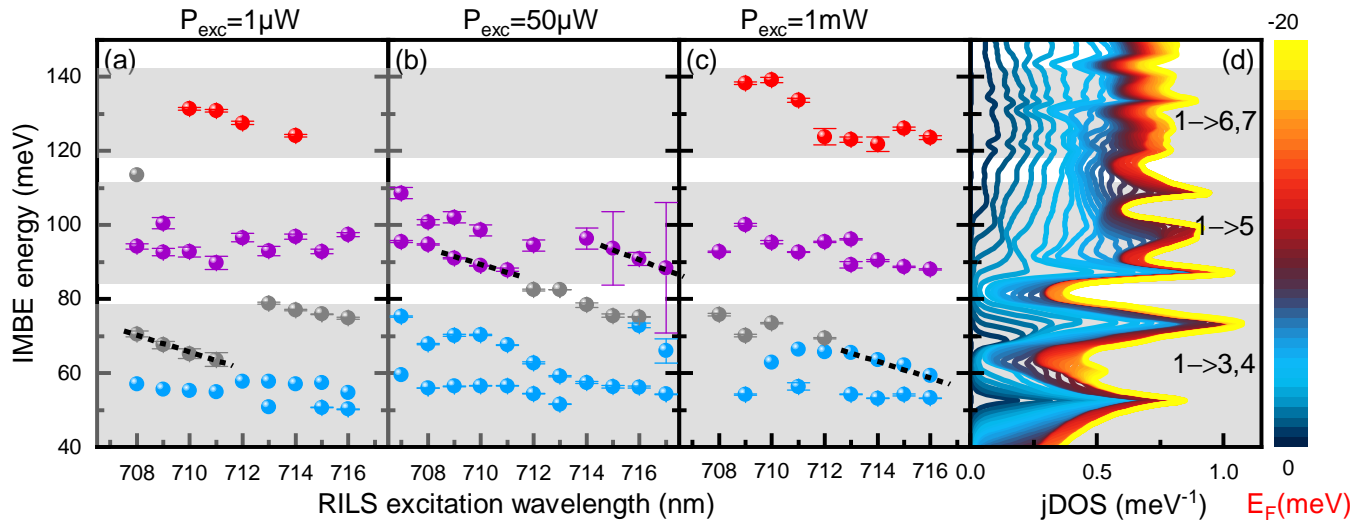


FIG. S4. Extracted peak energies from a line-shape analysis to the excitation power P_{Laser} dependent RILS measurements displayed in SI-Fig. S3 taken on the 3^o $tWSe_2$ bilayer at a temperature of $T = 4K$ at three different excitation powers of (a) $1\mu W$, (b) $50\mu W$ and (c) $1mW$, respectively. The corresponding changes in the photo-generated hole-densities are $\sim 10^9$ cm^{-2} , $\sim 10^{10}$ cm^{-2} and $\sim 10^{12}$ cm^{-2} , respectively. The lineshape analysis was performed as described in the main text by numerically describing the spectra fitting a suitable sum of Lorentzian curves to the spectra in order to deconvolute the dominating contribution to the spectra. Most of the peak energies of the Lorentz curves are constant by changing the excitation wavelength unambiguously identifying them RILS on collective excitations. The dashed lines mark data points where the RILS signal is likely superimposed by emission and hence slightly descend by increasing excitation wavelength. The combined fit error is in the order of a few percent. (d) Calculated joint density of states jDOS for IMB transitions in dependence of the Fermi-level E_F for 3^o $tWSe_2$ for vertical transitions.

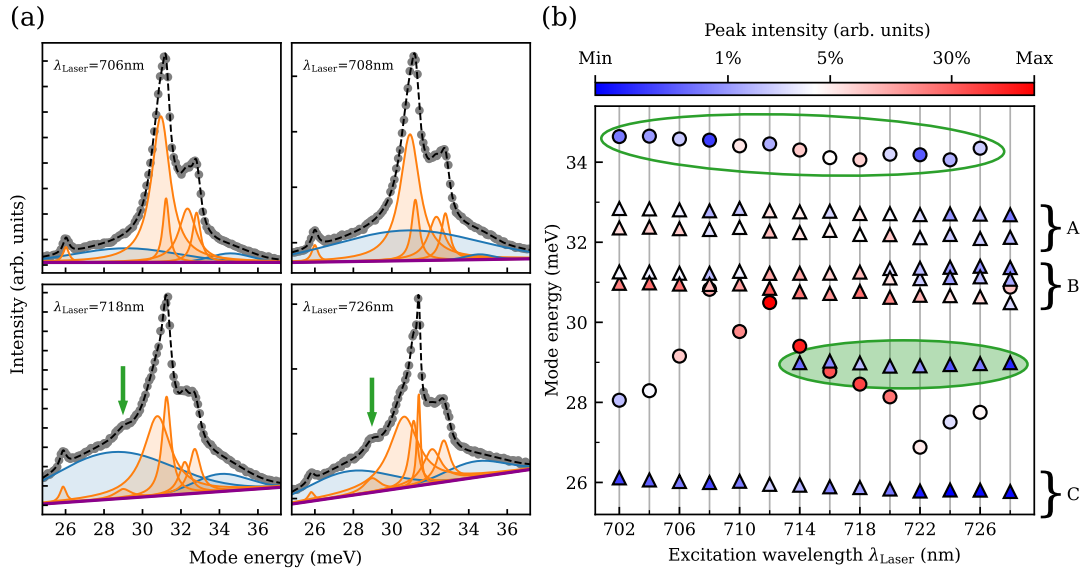


FIG. S5. (a) Example RILS spectra of the lower energy range between 24meV and 38meV (points) for the 3° tWSe₂ bilayer. The black dashed lines are the sum of a combination of Lorentz (orange) and Gauss (blue) curves in order to identify the individual contribution to the spectra after subtraction of a linear background (magenta). Overall, the described fit approach provides a very good numerical description of the experimental RILS spectra. In contrast to the higher energy range, we find a set of rather sharp modes that can be described by Lorentz terms in addition to one or two rather broad modes well described by Gaussian terms. The latter change with excitation wavelength and have similar absolute peak energies and are therefore assigned to PL. The relative energy shifts of the Lorentz curves are independent from the excitation wavelengths and are therefore assigned to inelastic scattering on collective excitations. Most of the Lorentz contributions are assigned to first order (Raman active) and second order Raman processes (enhanced by resonant excitation) by scattering on phonons in WSe₂. One mode at 28.8 meV cannot be assigned to phonon contributions and occurs only under extreme resonance. This mode is assigned to a collective IMBE between m_1 and m_2 moiré miniband. (b) Summary of the peak position as a function excitation wavelengths. The individual peak intensities are color coded using a logarithmic scale demonstrating the resonance conditions. Triangular data points are from Lorentzian fit curves assigned to inelastically scattered light due to their constant energy shifts and circular data are from Gaussian fit curves and are assigned to superimposed emission most likely due to defect-PL or in case of the signal being rather stable in energy for different excitation wavelength that might be also due to collective electronic excitations. The peak ensembles marked by A, B and C are interpreted as phonons. The RILS mode occurring at an energy of 28.8 meV only under extreme resonance in several set of data (not shown) for an excitation wavelength range for $714\text{nm} \leq \lambda_{Laser} \leq 728\text{nm}$ is interpreted as a collective electronic excitation. This mode is tentatively interpreted as IMBE between first and second moiré miniband $m_1 \rightarrow m_2$ in agreement with theory, but we cannot exclude an alternative interpretation as collective electronic excitation between the spin-split conduction bands $CB_- \rightarrow CB_+$ at the K points [see Fig.2 (a) in the main text]. For the assignment of the phonon modes we follow the combined experimental and theoretical work by Liam P. McDonnell and colleagues [S8] as follows. Region A: $E'_{LO}(K)$, $A'_1(K)$ or $2LA(M)$; Region B: $E'_{LO/TO}(\Gamma)$, $A'_1(\Gamma)$, $LA(M)+ZA(M)$; Region C (dispersing mode): $2TA(K)$ or $TA(M)+ZA(M)$;

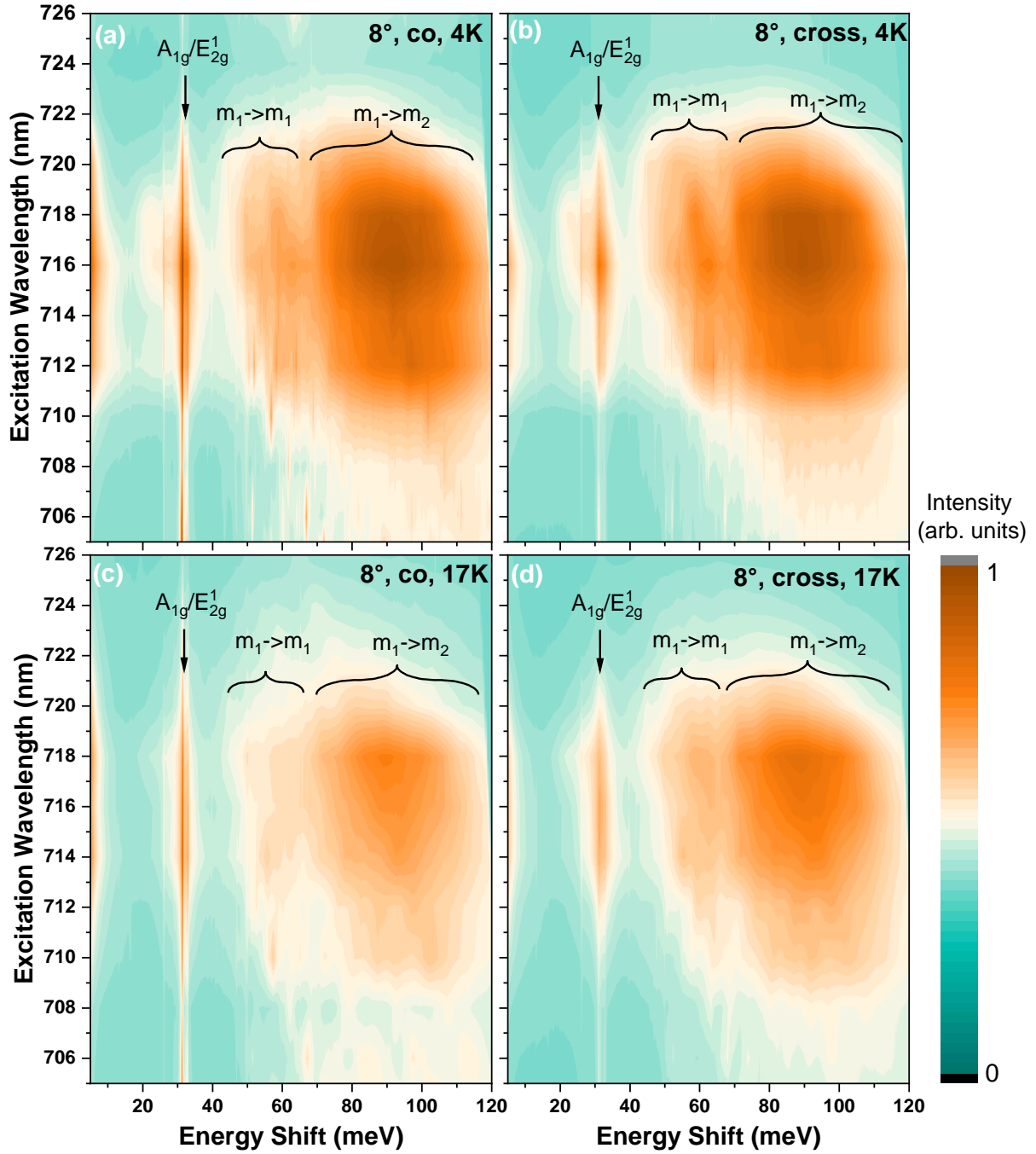
Temperature and polarization dependent RILS measurements on $tWSe_2$ ($t = 8$)

FIG. S6. False color representation of RILS spectra for 8° $tWSe_2$. Linear co- and cross scattering geometries are compared for two different temperatures. (a) co-polarized RILS spectra at $T = 4K$; (b) cross-polarized RILS spectra at $T = 4K$; (c) co-polarized RILS spectra at $T = 17K$; (d) cross-polarized RILS spectra at $T = 17K$ [$P = 500\mu W$]. The phonon modes and collective charge density excitations due to intra moiré band transitions $m_1 \rightarrow m_1$ as well as inter moiré band transitions $m_1 \rightarrow m_2$ are indicated. While we do not observe significant polarization dependence for the collective charge density excitation, those modes are smeared out by increasing the temperature from $4K$ to $17K$.

Calculated mini-band structure

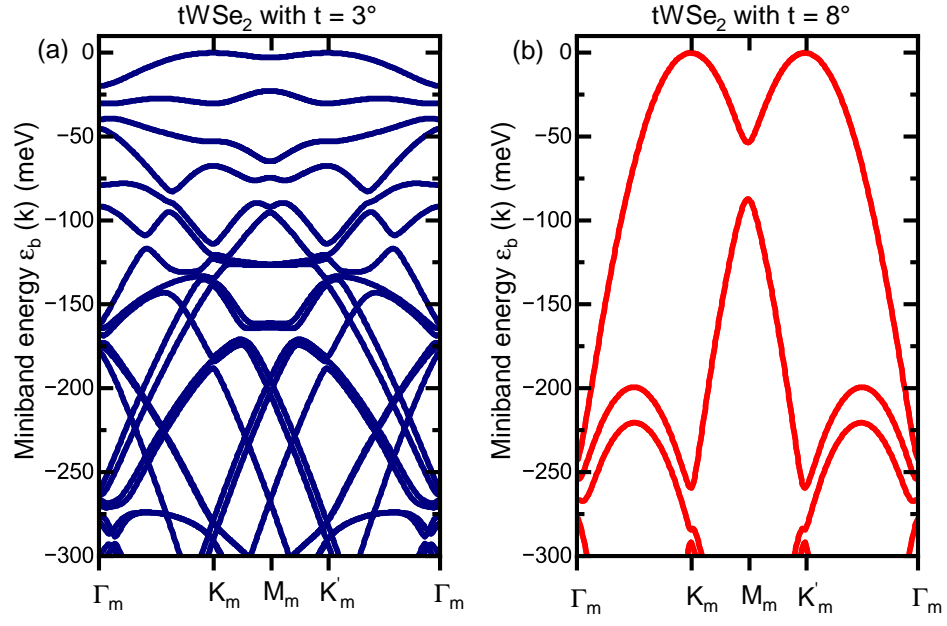


FIG. S7. Calculated energy dispersion of the highest moiré mini bands down to -300meV around the K, K' states for a 3° tWSe₂ bilayer (a) and a 8° tWSe₂ bilayer (b).

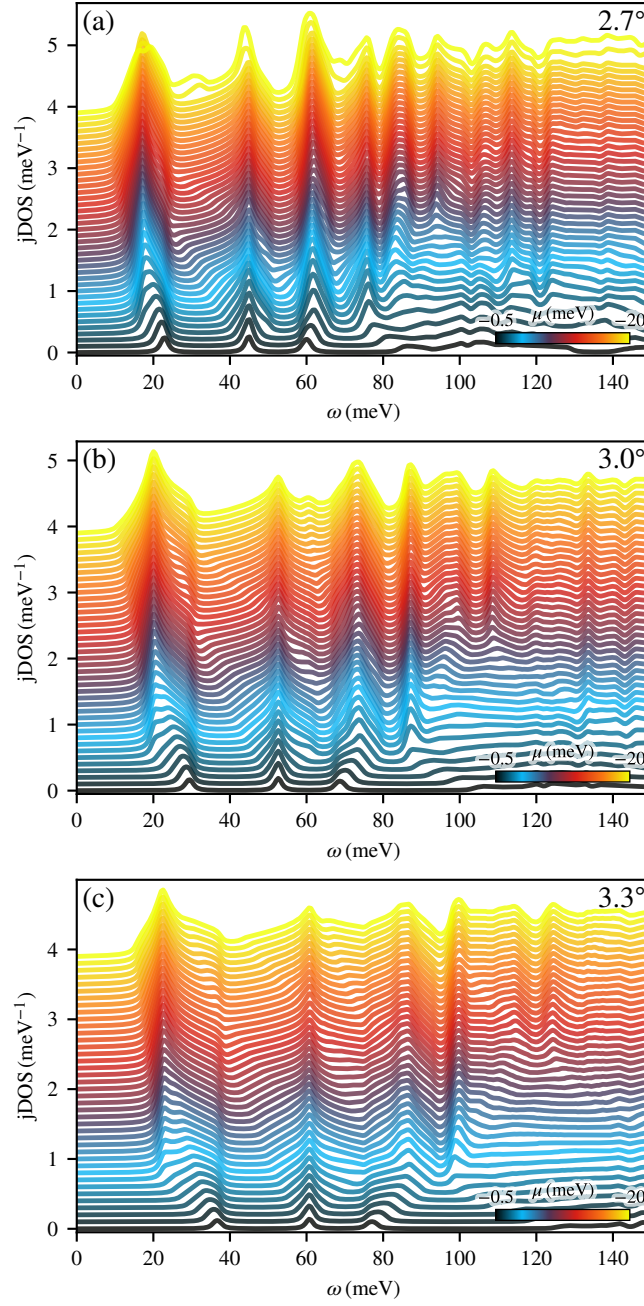
Calculated jDOS for $tWSe_2$ ($t = 3 \pm 0.3$)

FIG. S8. Calculated jDOS from the energy dispersion of the highest moiré mini bands the K, K' states for (a) 2.7° $tWSe_2$ bilayer (b) 3.0° $tWSe_2$ bilayer and (c) 3.3° $tWSe_2$ bilayer. The curves are offset by 0.1 meV^{-1} for clarity.

-
- [S1] G. Scuri, T. I. Andersen, Y. Zhou, D. S. Wild, J. Sung, R. J. Gelly, D. Bérubé, H. Heo, L. Shao, A. Y. Joe, A. M. Mier Valdivia, T. Taniguchi, K. Watanabe, M. Lončar, P. Kim, M. D. Lukin, and H. Park, Electrically tunable valley dynamics in twisted wse_2/wse_2 bilayers, *Phys. Rev. Lett.* **124**, 217403 (2020).
- [S2] F. Sigger, H. Lambers, K. Nisi, J. Klein, N. Saigal, A. W. Holleitner, and U. Wurstbauer, Spectroscopic imaging ellipsometry of two-dimensional TMDC heterostructures, *Applied Physics Letters* **121**, 071102 (2022), https://pubs.aip.org/aip/apl/article-pdf/doi/10.1063/5.0109189/16481539/071102_1_online.pdf.
- [S3] J. P. Bange, P. Werner, D. Schmitt, W. Bennecke, G. Meneghini, A. AlMutairi, M. Merboldt, K. Watanabe, T. Taniguchi, S. Steil, D. Steil, R. T. Weitz, S. Hofmann, G. S. M. Jansen, S. Brem, E. Malic, M. Reutzler, and S. Mathias, Ultrafast dynamics of bright and dark excitons in monolayer wse_2 and heterobilayer wse_2/mos_2 , *2D Materials* **10**, 035039 (2023).
- [S4] F. Wu, T. Lovorn, E. Tutuc, and A. H. MacDonald, Hubbard Model Physics in Transition Metal Dichalcogenide Moiré Bands, *Physical Review Letters* **121**, 026402 (2018).
- [S5] H. Pan, F. Wu, and S. Das Sarma, Band topology, Hubbard model, Heisenberg model, and Dzyaloshinskii-Moriya interaction in twisted bilayer WSe_2 , *Physical Review Research* **2**, 033087 (2020).
- [S6] T. Devakul, V. Crépel, Y. Zhang, and L. Fu, Magic in twisted transition metal dichalcogenide bilayers, *Nature Communications* **12**, 6730 (2021).
- [S7] S. Rye and T. O. Wehling, Switching between Mott-Hubbard and Hund Physics in Moiré Quantum Simulators, *Nano Letters* **23**, 573 (2023).
- [S8] L. P. McDonnell, J. J. S. Viner, P. Rivera, X. Xu, and D. C. Smith, Observation of intravalley phonon scattering of 2s excitons in $mose_2$ and wse_2 monolayers, *2D Materials* **7**, 045008 (2020).